Physics of the Earth and Planetary Interiors 194–195 (2012) 71–84

Contents lists available at SciVerse ScienceDirect

Physics of the Earth and Planetary Interiors

journal homepage: www.elsevier.com/locate/pepi

Exploring the potential of acquisition curves of the anhysteretic remanent magnetization as a tool to detect subtle magnetic alteration induced by heating

Lennart V. de Groot *, Mark J. Dekkers, Tom A.T. Mullender

Paleomagnetic Laboratory Fort Hoofddijk, Utrecht University, Budapestlaan 17, 3584 CD Utrecht, The Netherlands

ARTICLE INFO

Article history:
Received 5 August 2011
Received in revised form 29 December 2011
Accepted 12 January 2012
Available online 26 January 2012
Edited by Kei Hirose

Keywords:
Rock magnetism
Absolute paleointensity
Anhysteretic remanent magnetization
Thermochemical alteration

ABSTRACT

Recently, many new methods and improved protocols to determine the absolute paleointensity of lavas reliably have been proposed. Here we study eight recent flows from three different volcanic edifices (Mt. Etna, La Palma and Hawaii) with the so-called multispecimen parallel differential pTRM (MSP) method including the recently proposed domain-state correction (MSP-DSC) (Fabian and Leonhardt, 2010). Surprisingly, apart from approximately correct paleointensity values, we observe major underestimates of the paleofield. These deviations are possibly related to alteration that is not revealed by rock-magnetic analysis. We explore the potential of high-resolution acquisition curves of the anhysteretic remanent magnetization (ARM) to detect subtle alteration in the samples. It appears that assessing changes in the ARM acquisition properties before and after heating to the desired MSP temperature discriminates between underestimates and approximately correct estimations of the paleofield in the outcomes of the MSP-DSC protocol. By combining observations from the domain-state corrected MSP protocol and ARM acquisition experiments before and after heating, an extended MSP protocol is suggested which makes it possible to assess the best set temperature for the MSP-DSC protocol and to label MSP results as being approximately correct, or an underestimate of the paleofield.

1. Introduction

During the last decade several refinements of and alternative methods to the classic Thellier–Thellier-style paleointensity protocol (Thellier and Thellier, 1959; Coe, 1967) have been proposed (e.g. pTRM-tail checks (Riisager and Riisager, 2001); additivity checks (Krasa et al., 2003); the 'IZZI' protocol (Tauxe and Staudigel, 2004); microwave techniques (Hill and Shaw, 2000); single crystal analyses (Cottrell and Tarduno, 1999); the multispecimen approach (Dekkers and Böhnel, 2006; Fabian and Leonhardt, 2010) and the Wilson method (Muxworthy, 2010)). Most of these so called absolute paleointensity methods rely on heating samples to correlate the magnitude of imparted (partial) thermal remanent magnetizations ((p)TRMs) to natural remanent magnetizations (NRMs). Samples that are heated, however, are prone to alteration, either thermochemically or in their magnetic domain state. Using the correct temperature or range of temperatures in absolute paleointensity experiments to avoid these alterations is critical to the outcome. Determining this temperature or temperature range for which the paleointensity method yields the correct answer independently of the paleointensity experiment, if it exists, is a major challenge.

In this study we subjected samples from eight recent flows within the realm of the international geomagnetic reference field (IGRF) from three different volcanic edifices to detailed rock-magnetic analyses, assessing both high- and low-field magnetic properties as a function of temperature, before applying the domain-state-corrected multispecimen parallel differential pTRM (MSP) paleointensity method (Dekkers and Böhnel, 2006; Fabian and Leonhardt, 2010). The temperature used in the MSP paleointensity experiments does not indicate any alteration in the samples in the rock-magnetic analyses, however we find a range of paleointensity values from −42.6% to +5.5% of the appropriate IGRF value. Apparently the rock-magnetic analyses are not capable of diagnosing all possible alterations. Here we assess the potential of anhysteretic remanent magnetization (ARM) as an additional check for alteration as a consequence of laboratory heating. ARM is a remanence type that has a high resolving power for the small grains of interest here, in the single domain (SD) and small pseudo single domain (PSD) realms. Before and after heating, samples are given ARMs in increasingly stronger alternating fields generating detailed ARM acquisition curves enabling visualization of subtle changes in the samples.

2. Geological setting

Samples were collected from three different volcanic edifices: Mt. Etna, Italy (extensively studied to test various paleointensity

* Corresponding author. Tel.: +31 302535418.
E-mail address: l.v.degroot@uu.nl (L.V. de Groot).

0031-9201/$ - see front matter © 2012 Elsevier B.V. All rights reserved.
doi:10.1016/j.pepi.2012.01.006

Table 1
Site locations and reference data.

Site	Year	Latitude (N)	Longitude (E)	GPS error (m)	IGRF (dec)	IGRF (inc)	IGRF (int)
ET-23-2	1923	37°51′13.51″	15°6′51.19″	4	−5°40′	52°46′	42.3
ET-71-3C	1971	37°45′11.00″	15°5′12.59″	4	−0°38′	53°40′	43.9
ET-79-1	1979	37°44′26.77″	15°5′58.1″	5	0°20′	53°10′	44.1
ET-83-4A	1983	37°41′42.37″	14°59′28.15″	6	−0°26′	52°59′	44.2
LP-1	1949	28°36′4.05″	−17°53′14.91″	4	−14°32′	44°30	39.4
HW-14B	1955	19°23′56.28″	−154°55′8.82″	3	10°55′	36°55′	36.2
HW-17A	1960	19°30′25.44″	−154°50′27.78″	5	10°56′	37°11′	36.2
HW-37	1926	19°11′30.72″	−155°51′56.28″	4	10°16′	36°29′	36.6

From left to right: sites (ET = Etna, LP = La Palma, HW = Hawaii), ages (year AD), locations with GPS error and international geomagnetic reference field (IGRF) reference data (dec = declination; inc = inclination; int = intensity) for the sites used in this study.

methods (Tanguy, 1975; Hill and Shaw, 1999; Calvo et al., 2002; Speranza et al., 2006; Biggin et al., 2007a,b)); the 1949 eruption of Cumbre Vieja, La Palma, Canary Islands, Spain (Valet et al., 2010); and three sites on the 'Big Island', Hawaii, USA (Coe, 1978; Mankinen and Champion, 1993; Hill and Shaw, 2000; Yamamoto and Tsunakawa, 2003; Herrero-Bervera and Valet, 2009; Böhnel et al., 2011). GPS coordinates and full vector IGRF data of our sites are in Table 1; we briefly describe them below.

Here we use four sites of Mt. Etna: the 1923-flow, sampled at the Northwestern flank near the town of Linguaglossa (site 'ET-23-2'); the 1971 flow (site 'ET-71-3C') and the 1979-flow (site 'ET-79-1'), both sampled on the Eastern flank near the town of Fornazzo; and the 1983-flow, sampled on the Southern flank, North of Nicolosi. The 1923 and the 1971 flows were also studied by Hill and Shaw (1999); the samples of the 1979 and 1983 flows were taken near sampling sites of Biggin et al. (2007b). Those studies primarily used the microwave paleointensity technique and divided the samples in three groups based on rock-magnetic properties. Based on location and rock-magnetic properties, three of our Etna sites can be related to sites or samples from the aforementioned studies.

Site ET-71-3C can be associated with Hill and Shaw's sample 1971–9, which yielded a paleointensity of 39.8 μT, an underestimate of the expected value of 43.9 μT of 10%. Our site ET-79-1 can be related to Biggin et al.'s 1979 site, which yielded an average paleointensity of 42.6 μT, in good agreement with the expected IGRF value of 44.1 μT. Based on rock-magnetic properties we can relate site ET-83-4A to Biggin et al.'s 'L-type' 1983 samples, which generally yield underestimates of up to 25% of the expected paleointensity of 44.2 μT. Only site ET-23-2 cannot be reliably associated with either Hill and Shaw's sample 23-4 which yielded a paleointensity of 28.7 μT, or sample 23-8 which yielded 47.3 μT. The IGRF value for ET-23-2 is 42.3 μT.

Previous paleointensity studies on La Palma concentrated primarily on older events exposed in the Northeast of the island: the Matuyama–Brunes reversal (Brown et al., 2009; Valet and Soler, 1999) and a Miocene excursion of the geomagnetic field (Leonhardt et al., 2000). Valet et al. (2010) presented paleointensity results for sub-recent lava flows on La Palma. For this study, we sampled the 1949-flow erupted by the San Juan vent of the Cumbre Vieja volcano, near the village of Todoque, the IGRF value for this site ('LP-1') is 39.4 μT.

Of the three Hawaiian lavas included in this study, one – the Mauna Loa 1926 flow (site 'HW-37') – was sampled along the Hawaii Belt road at the Western side of the island of Hawaii. The other two flows are from the Kilauea volcano and were sampled on the Southeastern side of the island: the 1955 flow was sampled just South of the town of Kalani (site 'HW-14B') and the 1960 flow at the Eastern-most tip of the island (site 'HW-17A'). Both the 1955 and 1960 flows have been subject to several paleointensity studies, using samples from different sites from these flows and using different paleointensity techniques (Coe, 1978; Mankinen and Champion, 1993; Hill and Shaw, 2000; Yamamoto and Tsunakawa, 2003; Herrero-Bervera and Valet, 2009; Böhnel et al., 2011). The results of various paleointensity methods applied to the 1955 flow generally yield slight underestimates of the expected paleointensity of approximately 36 μT, but mostly within 10% of the expected value. For the 1960 flow, results from the aforementioned studies generally trend towards overestimates of the expected paleointensity, except for most results of the microwave technique (Hill and Shaw, 2000) which show slight underestimates. Our site HW-17A was sampled just centimeters apart from Yamamoto and Tsunakawa's (2003) samples B1-7. For this specific site they reported an average paleointensity of 58 μT (using the Coe–Thellier paleointensity protocol (Coe, 1967)), an overestimate of 60% with respect to the expected IGRF value.

Sites in this study were selected based on observed slight overestimates and severe underestimates from a larger data set containing sampled flows in the volcanic edifices of Mt. Etna, La Palma, and Hawaii. Although other sites from this data set were not subjected to such a detailed rock-magnetic analysis as the flows described in this paper, the sites presented here resemble typical behavior determined throughout the data set.

3. Methods

3.1. Sampling

Typically, 12–18 cores of 3–8 cm length and 2.5 cm diameter were drilled at each site, using a petrol-powered drill. At least eight samples per site were oriented, using both a magnetic and a sun compass. Where possible, sampling was done in fresh road-cuts. Solid parts of the flows were sampled, typically 0.5–1.5 m below the top of the massive part of the flow. The cores were taken just centimeters apart, to ensure as much homogeneity among the samples as possible.

3.2. Demagnetization of the NRM and rock-magnetic analyses

To assess the suitability for paleointensity experiments, first the samples' NRM was demagnetized both thermally and by alternating field (AF) demagnetization. Typically three specimens were processed thermally and 3–7 with AF demagnetization, per site. The thermal demagnetization experiments were done using a 2G DC-SQUID magnetometer (dynamic range 3×10^{-12}–5×10^{-5} Am^2, typical sample intensities were at the upper end of the dynamic range of the instrument) and an ASC TD48-SC thermal demagnetizer (residual field < 20 nT). The samples were generally demagnetized to above their maximum unblocking temperature in 10 temperature steps. The static three-axis AF demagnetization experiments were done with a robotized 2G DC-SQUID magnetometer (with the same specifications as mentioned above), with three orthogonal sets of AF demagnetization coils in line with the robot system. In up

to 20 field steps the samples were demagnetized down to a few percent of their NRM at 100 mT.

These experiments also served to select a suitable temperature for the MSP paleointensity experiments (from now on referred to as the 'set temperature'): a significant amount of the NRM should be demagnetized at that temperature, while avoiding chemical alteration of the samples. To assess the chemical alteration temperature the samples were subjected to thermomagnetic analysis in air with a modified horizontal translation Curie balance (Mullender et al., 1993). The magnetization was measured as a function of temperature during several temperature cycles up to increasingly elevated temperature (heating and cooling rate 10 °C/min). Furthermore the magnetic susceptibility of the samples was measured as a function of temperature on an AGICO KLY-3S susceptometer with a CS-3 furnace attachment (measurement frequency 976 Hz, field strength 400 A/m peak level, noise level 2×10^{-7} SI, typical signal at least 3 orders of magnitude higher). Analysis was done in air with a 'medium' heating rate implying heating and cooling of ~10 °C/min. Again, the samples were subjected to several temperature cycles to increasingly higher temperature. The highest temperature reached in the last thermal cycle that shows reversible behavior, during both the magnetization and susceptibility versus temperature runs, will be referred to as the 'alteration temperature' of that sample. It is considered the highest temperature that can be used in paleointensity experiments.

To get insight in the magnetic domain state of the flows, at least three samples per site were used to assess the high-field rock-magnetic properties on a Princeton instruments alternating gradient force magnetometer (PMC Model 2900, instrumental noise level < 2×10^{-9} Am^2, typical signals at least 4 orders of magnitude higher). Both hysteresis loops (maximum field 1 T) and back-field remanence curves were measured to obtain all parameters needed for a so-called Day-plot: saturation magnetization (M_s), remanent saturation magnetization (M_{rs}), coercive force (B_c) and remanent coercive force (B_{cr}).

3.3. Paleointensity determination

For the determination of the paleointensity the MSP-DSC protocol was used (Dekkers and Böhnel, 2006; Fabian and Leonhardt, 2010). In the classical MSP paleointensity method (Dekkers and Böhnel, 2006) an in-field heated pTRM is imparted in several sister samples using different DC fields aligned parallel to the NRM of the sample. All samples are heated to the same temperature and are treated just once. The DC field for which the pTRM is equal to the NRM of the sample is considered to be the paleofield. To determine this DC field, the ratio of the pTRM to the NRM is calculated per sample: (pTRM-NRM)/NRM. These ratios are plotted as a function of the DC field used for that sample, the field strength for which the linear fit to the data intersects the *x*-axis (where (pTRM-NRM)/NRM changes sign) is the estimated intensity of the paleofield. To have a well defined intersection of the fitted line and the *x*-axis, a comparatively steep-sloped line fit with a reasonably narrow uncertainty envelope is desirable, since the percentage of the NRM that is removed at the set temperature used in the experiment largely determines the slope of the fit in the MSP plot, it is important to choose a set temperature for which a sufficient amount of the NRM is removed.

Recently, Fabian and Leonhardt (2010) showed experimentally that the original claim of domain-state independence by Dekkers and Böhnel (2006) was not entirely correct. Furthermore, the classical MSP protocol suffers from tail effects associated with imparting a pTRM. Fabian and Leonhardt (2010) proposed an addition to the classic MSP protocol to correct for these tail- and potential domain-state effects. Their extended protocol includes three extra heating steps to quantify potential tail effects introduced while imparting the pTRM during the MSP experiment (note that the first step is equal to the MSP experiment of Dekkers and Böhnel (2006)). The phenomenological model of Fabian and Leonhardt (2010) predicts that these tail effects always lead to an overestimate of the paleointensity in the classical MSP protocol. Although the three extra heating steps (step 2 with the DC field applied antiparallel to the NRM; step 3 heating in zero-field, cooling with the DC field applied parallel to the NRM; and step 4 a repeat of the first heating step of the experiment, with the field applied parallel to the NRM of the sample) introduce potential bias due to magnetic treatment history, the experiments of Fabian and Leonhardt (2010) on synthetic samples of different grain sizes yield very good results. We applied the extended protocol (further referred to as MSP-DSC, in which DSC stands for 'domain state corrected') to our sites, with the fraction α (Fabian and Leonhardt, 2010) set to 0.5. Following the nomenclature of Fabian and Leonhardt (2010), the classical MSP protocol is further referred to as 'MSP-DB'.

Depending on the percentage of NRM lost at the set temperature for the MSP-style experiments and the r^2 of the fit, between 5 and 27 samples were used in the paleointensity experiments. To express how well the paleointensity resembles the IGRF intensity, the intensity error fraction (IEF) was calculated for all sites. The IEF is given by the difference between the obtained and expected paleointensity expressed as a percentage of the expected paleointensity (Biggin et al., 2007a). All measurements needed for the paleointensity protocols were done on either the aforementioned 2G DC SQUID magnetometer or an AGICO JR-6 spinner magnetometer (sensitivity 2×10^{-6} A/m at high speed, typical signal strength 3 orders of magnitude higher).

3.4. ARM acquisition experiments

3.4.1. Rationale

As we will see in Section 4, the outcome of the MSP-DSC paleointensity protocol using the set temperature for which the rock-magnetic analyses described above indicate no changes in magnetic behavior of the samples yields approximately correct paleointensities, slight overestimates and major underestimates with respect to the IGRF. This implies that the rock-magnetic analyses described above are not fully capable of detecting all possible alterations in the samples. Further, changes in domain configuration are difficult to surmise with magnetization or susceptibility versus temperature experiments. Hysteresis parameters are somewhat biased in favor of the large particles which are less prone to alter. Initial alteration like incipient oxy-exsolution, involves small particles. Intermediate titanomagnetite may exsolve into a magnetite-rich and ulvöspinel-rich endmember as a consequence of laboratory heating during a paleointensity experiment (Dunlop and Özdemir, 1997).

In order to get a more complete picture of potential alteration we explore the potential of ARM acquisition curves. Mass-specific ARM shows substantial changes as function of grain size particularly in the PSD-SD size realm. Thus, it may be a sensitive probe to diagnose incipient alteration.

ARM has been used as analog for TRM although its theoretical basis is rather weak. The Lowrie–Fuller test (Lowrie and Fuller, 1971; Xu and Dunlop, 1995) which compares IRM and TRM coercivity spectra as a domain state indicator and the modified Lowrie–Fuller test (Johnson et al., 1975), which compares ARM and IRM coercivity spectra with the same purpose, yield broadly similar information. ARM and TRM are both low-field remanences and AF demagnetization spectra of TRMs and ARMs of sister samples are similar, in terms of intensity as well as coercivity properties.

Further up to the low fields of interest TRM is proportional to the inducing field and ARM proportional to the DC bias field. Many

relative paleointensity studies take ARM as their preferred normalizer for these reasons (e.g. Meynadier et al., 1992; Valet and Meynadier, 1993; Yamazaki et al., 2008; Inoue and Yamazaki, 2010).

The analogy between ARM and TRM is also used in the Shaw-family of paleointensity experiments where ARM measurements are incorporated in the assessment of the paleointensity, avoiding the need of heating samples multiple times as in Thellier style experiments (Shaw, 1974; Kono and Ueno, 1977; Rolph and Shaw, 1985; Tsunakawa and Shaw, 1994; Yamamoto and Tsunakawa, 2003). In Shaw-type paleointensity experiments the coercivity spectra of the NRM and the saturated ARM of the samples are assessed, prior to imparting a full TRM in a known magnetic field on the samples. Then the coercivity spectra of the full TRM and subsequently the coercivity spectrum of a saturated ARM of the heated specimens are assessed. If the coercivity spectra of the saturated ARMs before and after heating do not match, the paleointensity obtained through the NRM/TRM ratio is suspect.

If the ARM acquisition relates to the TRM as presumed above, samples that acquire more ARM after heating are expected to acquire more pTRM during the paleointensity experiment. Then in the MSP paleointensity experiment, for a given field strength the (pTRM-NRM)/NRM ratio is too high which would yield an underestimate of the paleointensity of the field. Vice versa, samples that acquire less ARM after heating are expected to yield a too low paleointensity ratio and thus an overestimate. No change in the acquisition curve of the ARM implies that the acquisition properties for ARM/pTRMs do not change, and that the MSP paleointensity ratio should yield (approximately) the correct paleointensity.

3.4.2. ARM acquisition starting from the AF demagnetized magnetic state

If the NRM is fully demagnetized before the ARM acquisition experiments, we can directly measure the ARM acquisition curve. We treat the samples with an AF demagnetization field of 300 mT in three axis, with the last axis along the direction of the DC field of the ARM acquisition experiment. Rather than relying on one ARM value, for example the saturation ARM acquired in a high AF, we utilize the robotized magnetometer set-up with which it is straightforward to measure a detailed ARM acquisition curve across the entire AF range from 0 to 150 mT. All samples are subjected to 26 increasing AF fields in the presence of a 35 μT DC field. To assess potential small-scale differences in concentration and/or magnetic properties within the same flow, four samples are subjected to the ARM acquisition experiment and the data series are normalized to the mass of the samples. Averaging the normalized data series per AF field step yields the ARM acquisition curve. We refer to the ARM acquisition experiment on AF demagnetized samples as the 'ARM acquisition of the AF demagnetized state'.

3.4.3. ARM acquisition starting from the NRM magnetic state

The procedure just outlined is a rather straightforward way of measuring an ARM acquisition curve. However, possible subtle changes in domain state that could be introduced by the heating of the sample in the paleointensity experiment pose a problem. They may be a cause of the under- and overestimates of the paleointensities observed. AF demagnetization prior to the ARM acquisition may affect or even fully remove their detection.

To assess the ARM acquisition of pristine samples in their NRM magnetic state, we should realize that for each field level ARM is induced but at the same time NRM is demagnetized by single-axis AF demagnetization (i.e. along the ARM acquisition axis). Here we present two measurement protocols to separate the ARM acquisition from the NRM demagnetization. The first protocol mathematically separates the ARM acquisition from the demagnetizing NRM by aligning half of the samples parallel to the DC field used in the ARM acquisition experiment and the other half of the samples antiparallel to that field. This experiment will be referred to as the 'aligned ARM acquisition' (AL) experiment. The second experiment makes use of multiple specimens cut from one drilled core, assuming that the direction of the NRM with respect to a fiducial marking in the length of the core and the specific NRM of all specimens from one core is (approximately) equal. This second experiment is referred to as the 'single core ARM acquisition' (SC) experiment.

Both experiments described above implicitly assume that demagnetizing the NRM and acquiring an ARM are independent processes, which need not to be the case. However, both techniques of removing the NRM prior to an ARM acquisition (AF and thermal demagnetization) are prone to alter the magnetic state of the samples.

3.4.3.1. Aligned ARM acquisition. The samples with their NRM direction aligned parallel to the DC field acquire the ARM in the same direction as their NRM is removed. The measured vector per AF field step is the sum of the (partially) demagnetized NRM and the acquired ARM. The samples that were aligned antiparallel to the DC field, acquire the ARM in the opposite direction as their (partially) demagnetized NRM. The measured vector per AF field step is the difference between the (partially demagnetized) NRM and the acquired ARM. For both groups of samples the data series are made mass specific and are averaged. Now we can mathematically extract the curves of the remaining NRM and the acquired ARM by the following formulae (Fig. 1a):

$$\overline{\mathrm{NRM}_{\mathrm{remaining}}} = \frac{\overline{M_{\mathrm{p}}} - \overline{M_{\mathrm{ap}}}}{2}$$

$$\overline{\mathrm{ARM}_{\mathrm{acquired}}} = \frac{\overline{M_{\mathrm{p}}} + \overline{M_{\mathrm{ap}}}}{2}$$

in which M_{p} is the average measured vector of the parallel group and M_{ap} the average measured vector of the antiparallel group of samples.

In the aligned ARM acquisition experiment the samples need to be aligned to their NRM within the limited space of the sample holder of the robotized magnetometer. Therefore only very small samples, typically between 0.2 and 1 g, can be used. Because of potential inhomogeneity of the sample material, at least four samples per direction, so eight samples in total are needed for a reliable ARM acquisition curve. All samples are subjected to a high-resolution ARM acquisition curve, with 46 AF steps between 0 and 150 mT using the robotized 2G SQUID magnetometer. Sixteen of those steps are selected between 0 and 10 mT to acquire a detailed view of what occurs in the vicinity of the magnetic starting state of the experiment.

Preliminary experiments have shown that the variation of the specific NRM can be much larger than the variation of the full specific ARM for the small samples used in the aligned ARM experiments (compare the variation at low and high AFs in Fig. 2a). If the magnitude of the specific NRM of the group of parallel aligned samples and the group of antiparallel aligned samples are not approximately equal due to scatter in the specific NRM per sample, the formula for $\mathrm{ARM}_{\mathrm{acquired}}$ does not yield 0 $\mathrm{Am}^2/\mathrm{kg}$ for the measurement of the pristine NRM (Fig. 2b) and are thus biased by the scatter in the NRM. Here we introduce a method to correct for the scatter in the $\mathrm{NRM}_{\mathrm{remaining}}$, without introducing bias in the $\mathrm{ARM}_{\mathrm{acquired}}$ for high AF fields.

Since the NRM dominates the measurements for the low AF fields and the full ARM governs the data series for the high AF fields of the ARM acquisition experiment, we cannot correct the data using either the average specific NRM or the average full specific ARM, without biasing the other end of the data series. If the behavior of the demagnetizing specific NRM is known, we could use that

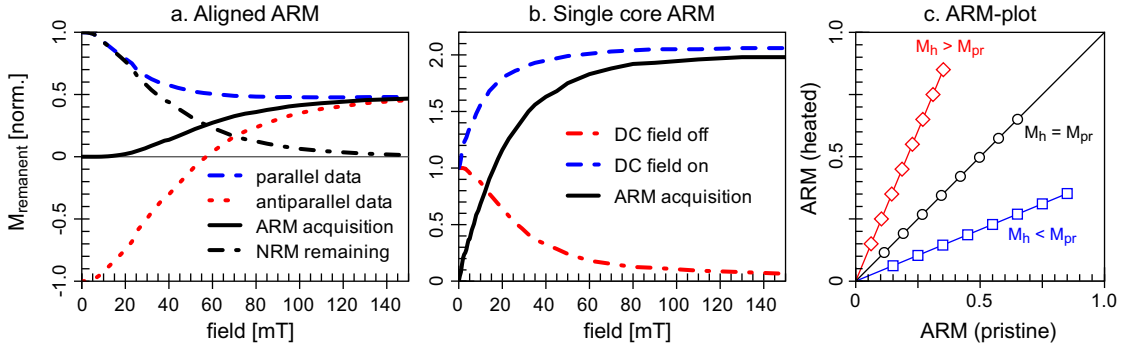

Fig. 1. ARM acquisition plots. (a) Aligned ARM acquisition experiment. The ARM acquisition is the average of the parallel and the antiparallel data; the NRM demagnetization is obtained by subtracting the antiparallel data from the parallel data and dividing the result by two. (b) Single core ARM acquisition experiment: the ARM acquisition is obtained by subtracting the data series from the ARM acquisition with the DC field switched off from the data series of the ARM acquisition with the DC field switched on. (c) ARM-plot. Samples plotting on the $x = y$ diagonal (black circles) acquire the same ARM before (M_{pr}) and after heating (M_h). Samples plotting below the diagonal (blue squares) acquire less ARM after heating. Samples plotting above the diagonal (red diamonds) acquire more ARM after heating. The latter would yield paleointensity underestimates while samples plotting below the diagonal would yield paleointensity overestimates. (For interpretation of the references to color in this figure legend, the reader is referred to the web version of this article.)

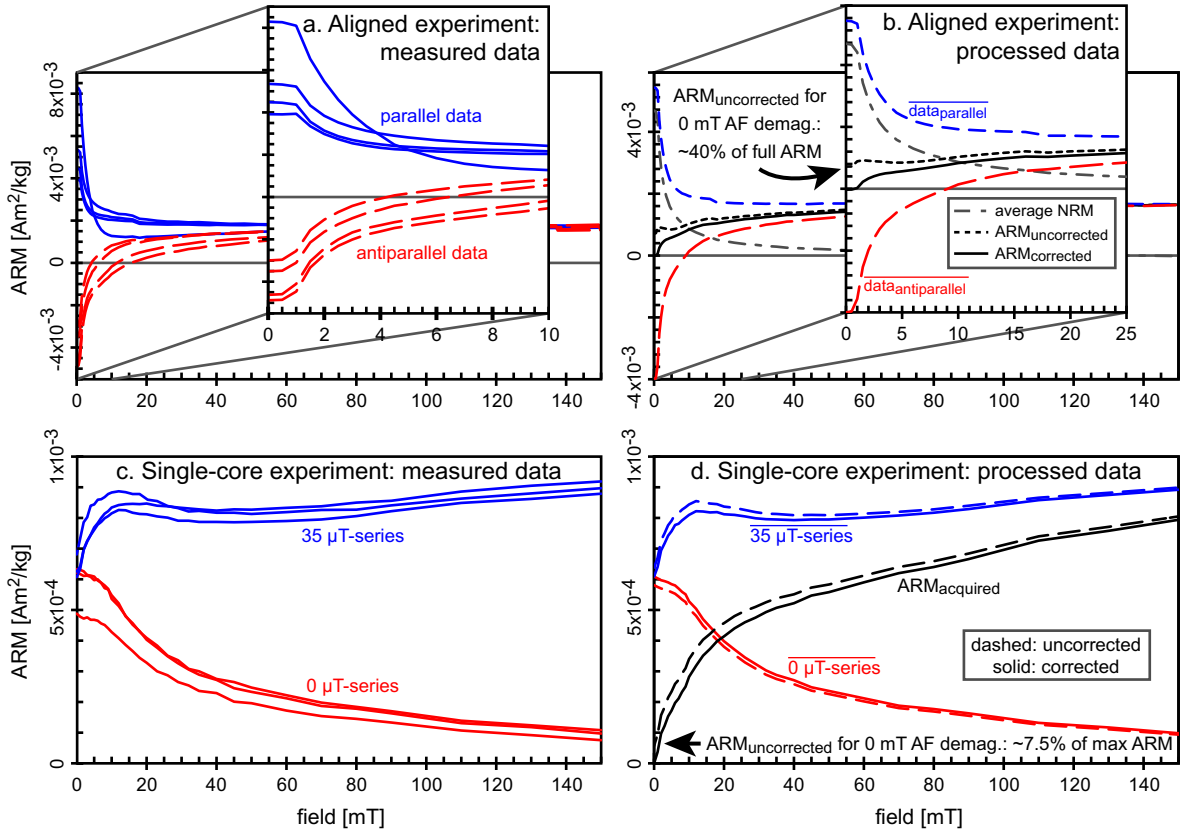

Fig. 2. (a) Results of an aligned ARM experiment with small samples (0.2–1 g), the DC bias field is applied in the positive direction. Samples are from ET-79-1. Blue solid lines: four samples aligned parallel to the applied DC bias field in the ARM acquisition. Dashed red lines: four samples aligned antiparallel to that field. (b) The processed data of the experiment of the data in (a): without the NRM scatter correction the ARM acquisition starts at approximately 40% of the full ARM. (c) Single-core ARM acquisition experiment using large samples (8–12 g) with the DC field applied in the negative direction. Blue lines towards the top-right corner are the 35-µT-series, red lines towards the bottom-right corner of the panel are the 0-µT-series. Samples are from HW-17A. (d) Processed data of the experiment in panel (c): the uncorrected lines are dashed; the solid lines are the NRM scatter corrected data. The data in the SC experiment are less sensitive to corrections for the NRM scatter, likely due to the bigger samples used in that experiment. (For interpretation of the references to color in this figure legend, the reader is referred to the web version of this article.)

to apply a gradual correction depending on which effect, the $NRM_{remaining}$ or the $ARM_{acquired}$, dominates the measurement for each AF field used in the ARM acquisition experiment. Therefore we define a NRM weight factor, a, by scaling the average $NRM_{remaining}$ between 0 and 1, as follows:

$$a = \left[\frac{\overline{M_p} - \overline{M_{ap}}}{2}\right]_0^1$$

This parameter indicates whether the NRM ($a = 1$) or the full ARM ($a = 0$) dominates the measured vector for each AF field used in the ARM experiment.

If we now apply the normalization parameter to the formula of the $ARM_{remaining}$ per AF field step, the error due to scatter in the NRM is removed from the $ARM_{acquired}$ (Fig. 2b):

$$\overline{ARM_{acquired,corr}} = \frac{(\overline{M_p} + \overline{M_{ap}})(1 - a)}{2}$$

The mathematical derivation of the proposed correction is treated in full in the Supplementary material.

3.4.3.2. Single-core ARM acquisition. In the single-core ARM acquisition experiment, a drill core is marked with a fiducial line, before the core is cut in an even number of specimens with a diameter of 2.5 cm and approximately 1 cm thick, ranging between 8 and 12 g. There are no requirements concerning NRM and ARM directions which makes the single-core ARM acquisition experiment less demanding than the aligned ARM acquisition experiment. This applies to the need of having dedicated holders for orientation; some instrument time is saved. It, however, requires more sample material.

All specimens from the core are subjected to an ARM acquisition with respect to the fiducial line, using up to 36 steps in increasing intervals between 0 and 150 mT. For half of the core's samples, however, the DC bias field of the ARM acquisition is set to zero, so we actually conduct a single axis AF demagnetization along the direction of the ARM acquisition. Normalizing the measurements for each sample to its respective mass followed by averaging the data per AF level for all samples yields the behavior of the single axis AF demagnetization of the specific NRM; we will refer to this data series as the '0-μT-series'. The other half of the specimens are given an ARM acquisition with respect to the fiducial line, with the DC field of the ARM acquisition set to 35 μT. The data series of this second group of specimens are also normalized to the specimen's mass and averaged per AF level for all specimens; this yields a combined signal of the ARM acquisition due to the DC bias field of 35 μT and the demagnetizing NRM; this data series will be referred to as '35-μT-series'. The $ARM_{acquired}$ is given by (Fig. 1b):

$$\overline{ARM_{acquired}} = \overline{M_{35\,\mu T\text{-series}}} - \overline{M_{0\,\mu T\text{-series}}}$$

Although the scatter of the specific NRM is likely less significant for the large sample size used in the single core experiment than for the small samples used in the aligned ARM acquisition experiment (compare Fig. 2a and c), preliminary experiments indicated that it is still useful to correct for the scatter in the specific NRM. The mathematical derivation of this correction is treated in depth in the Supplementary material. To correct the 0-μT-series and the 35-μT-series such that the average specific NRM for both series becomes the average value of the specific NRM of the two series, we define a scale factor, *b*, as follows:

$$b = \sqrt{\frac{\overline{NRM_{0\,\mu T}}}{\overline{NRM_{35\,\mu T}}}}$$

In which $NRM_{0\,\mu T}$ is the average specific NRM of the 0-μT-series and $NRM_{35\,\mu T}$ is the average specific NRM of the 35-μT-series. Since the samples in the 0-μT-series did not acquire an ARM, but underwent single axis AF demagnetization, we can normalize the series by *b*, without considering the differences in scatter between the specific NRM and the specific ARM. The normalized 0-μT-series is thus given by:

$$\overline{M_{0\,\mu T,corr}} = \frac{\overline{M_{0\,\mu T}}}{b}$$

For the 35-μT-series, however, the differences in variation between the NRM per mass and the ARM per mass need to be taken into account, since correcting the full series for the scatter in the NRM would introduce bias in the part of the series where the full ARM dominates the signal. As in the aligned ARM acquisition experiment, we use the NRM weight factor, *a*. In the single-core ARM acquisition experiment the NRM weight factor can be obtained directly from the 0-μT-series, since this experiment *de facto* is a single axis AF demagnetization. Normalizing this series between 0 and 1 yields *a*:

$$a = [\overline{M_{0\,\mu T}}]_0^1$$

Now we can normalize the 35-μT-series such that the scatter in the specific NRM is suppressed, without biasing the ARM acquisition in the samples, by:

$$\overline{M_{35\,\mu T,corr}} = ab\overline{M_{35\,\mu T}} + (1-a)\overline{M_{35\,\mu T}}$$

In which the middle term is the 35-μT-series, normalized for the scatter in the specific NRM, weighted to the influence of the specific NRM on the signal for each AF step used; the last term is the uncorrected 35-μT-series, weighted to the influence of the ARM acquired for increasing AF fields used. The $ARM_{acquired}$ is now given by:

$$\overline{ARM_{acquired,corr}} = \overline{M_{35\,\mu T,corr}} - \overline{M_{0\,\mu T,corr}}$$

The samples ideally should be isotropic because the ARM intensity is compared to the NRM intensity independent of differences in NRM and ARM direction. In contrast to some pottery shards and kilns lavas are not very anisotropic. Anisotropy of the low-field susceptibility indicated values for the total anisotropy between 1% and 3%, so gross differences among samples because of directional differences are not anticipated.

In an equal area-plot of the 35-μT-series (not shown here) the data points per AF step of the ARM acquisition trend from the NRM direction with respect to the fiducial line towards the direction of the ARM that is induced during the experiment. If we assume independency between demagnetizing the NRM and acquiring the ARM, this change in direction during the experiment can be fully attributed to the demagnetizing NRM. The influence of a thermal demagnetization step before the single core ARM acquisition experiment is removed similarly: the effect of such a demagnetization step is equal for both groups of samples used in the experiment and is thus removed from the ARM acquisition by subtracting the 0-μT-series from the 35-μT-series.

3.4.4. Evaluation of changes in the samples

Once the ARM acquisition curves are isolated for both pristine and heated samples, we can plot the results for each field step with the ARM acquisition of the pristine samples on the *x*-axis and the results of the heated samples on the *y*-axis (Fig. 1c). If the ARM acquisition for the heated samples is equal to the ARM acquisition of the pristine samples, the data would plot on the line $x = y$ in the ARM-plot. If the samples acquire more ARM after heating, the data plot above the line $x = y$, if the samples acquire less ARM after treatment, the data will be below the line $x = y$. When the samples saturate and the ARM does not increase anymore, the data points cluster at the saturation ARM.

4. Results

4.1. AF and thermal demagnetization of the NRM

Typical NRM signals are approximately $2–4 \times 10^{-3}$ Am^2/kg for all sites (Fig. 3). NRMs all trend linearly towards the origin in Zijderveld diagrams (Fig. 3a1–a8 and c1–c8). NRM overprints, if present at all, deviate only a few degrees from the characteristic NRM component. They are already removed by 2.5 mT AF demagnetization or by thermal demagnetization at less than 100 °C. The NRM is reduced to 5% of its starting value after AF demagnetization at 100 mT; except for HW-17A and HW-37 in which ~25% is left at 100 mT. Thermally, the NRM is fully removed at 580 °C for all samples.

The AF decay curves of the NRM (Fig. 3b1–b8) appear to be broadly similar for all eight sites, although sites ET-71-3C and ET-79-1 loose more of their NRM for lower AF fields. Thermal decay curves of the NRM (Fig. 3d1–d8) show more variation

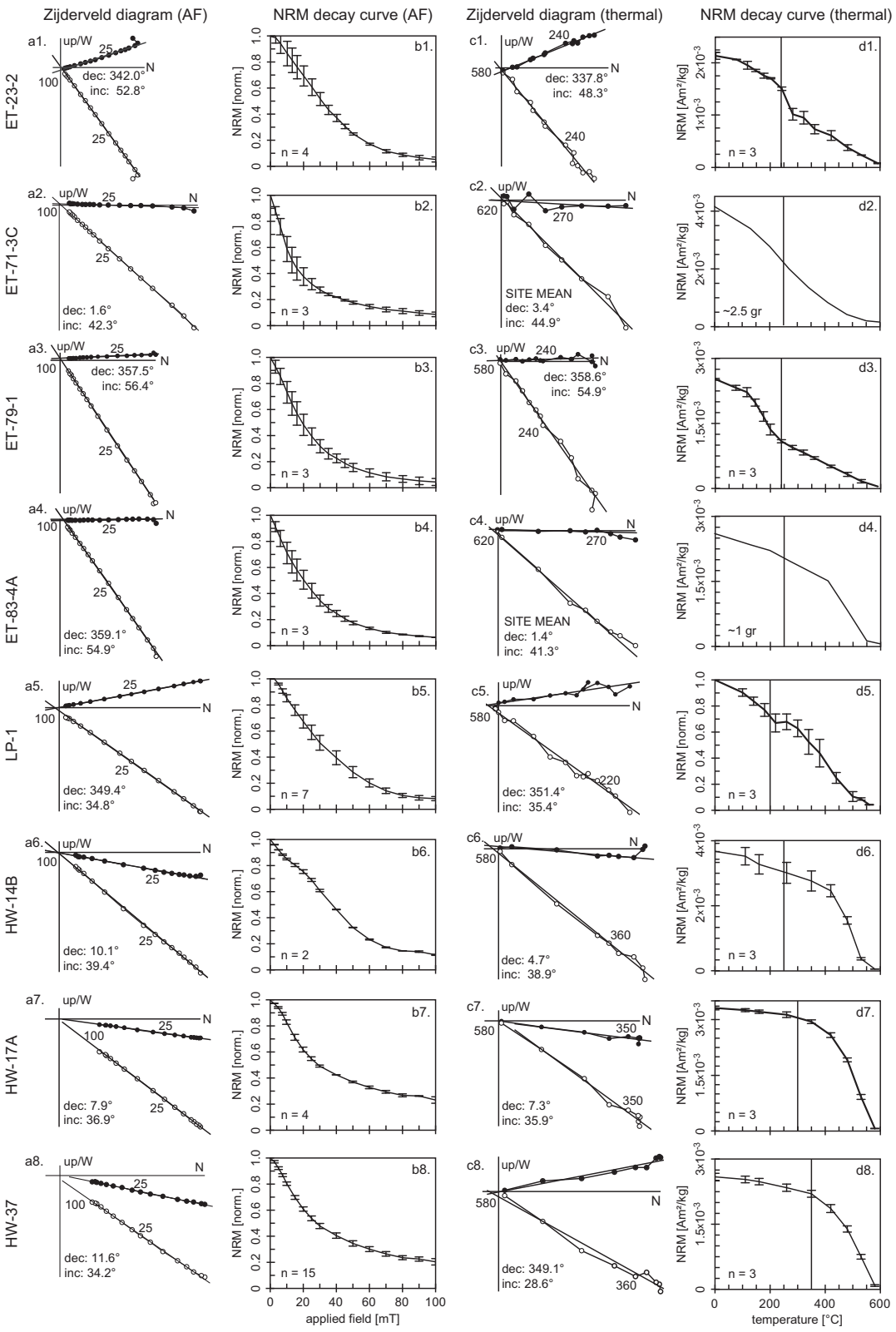

Fig. 3. NRM demagnetizations, for sample labels see Table 1. Typical Zijderveld plots (a1–a8 and c1–c8) and NRM decay curves (b1–b8 and d1–d8), for both AF (a and b) and thermal demagnetization (c and d). Samples show univectorial behavior towards the origin. No or very small overprints are present in the samples. If present, overprints are removed by the first demagnetization step. The thermal demagnetization curves of sites ET-71-3C and ET-83-4A (panels c2 and c4) were acquired from unoriented samples, the data is plotted such that the average direction is approximately equal to the site mean direction of the AF demagnetized samples. In the decay curves the number of samples used for calculating the average behavior is indicated, error bars for each demagnetization level are one standard deviation above and below the average. All AF NRM decay curves and the thermal decay curve of LP-1 (La Palma) are normalized to their starting NRM, introducing relatively large errors in the steeper parts of the decay curve. The thermal NRM decay curves of the Etna (ET) and Hawaii (HW) sites are mass normalized, yielding less scatter in the average. The MSP set temperature is indicated in the thermal NRM decay curves as the vertical solid black line.

between the sites. For the Etna and La Palma sites a relatively gradual decay of the NRM towards 580 °C is observed. The Hawaiian sites keep a major portion of their NRM up to higher temperatures: generally ~75% of their NRM is demagnetized between 400 and 580 °C. This indicates that these Hawaiian lavas contain a large portion of non-substituted magnetite. Except for site ET-23-1, both AF and thermal characteristic NRM directions are generally in good agreement with the expected directions from the IGRF for the location and age of the samples (Table 1).

4.2. Hysteresis loop parameters and thermal analyses

The hysteresis loops reveal PSD behavior for all sites (Fig. 4a1–a8). M_s of the Etna and La Palma sites is approximately 2 Am^2/kg, that for the Hawaiian sites is approximately 1 Am^2/kg. In comparison to the other samples, the branches of the hysteresis loops of ET-71-3C and ET-79-1 are closer together, implying more MD-like behavior. Sites LP-1 and HW-14B show a more pronounced SD-like behavior. In a Day plot (Day et al., 1977) of M_{rs}/M_s versus B_{cr}/B_c (Fig. 4b1–b8) all samples plot with in the PSD realm, with indeed ET-79-1 trending most towards the MD area and HW-14B trending most towards the SD area. The data of the Hawaiian samples and ET-71-3C reveal the least scatter.

All sites except ET-71-3C and ET-79-1 show a dominant Curie temperature of 550 °C (Fig. 4c1–c8), just below the Curie temperature of pure magnetite (Dunlop and Özdemir, 1997). In contrast to the behavior of pure magnetite, all sites show a relatively gradual decay of the magnetization with temperature, indicating a broad distribution of grains with different titanium–iron ratios. ET-71-3C and ET-79-1 reveal a low Curie temperature of approximately 280 °C, indicating a more titanium-rich titanomagnetite composition than the other sites.

Thermochemical alteration in our samples is best illustrated by the results of susceptibility-versus-temperature runs; apparently chemical alteration is revealed by the susceptibility of the sample quicker than by its magnetization. For all sites from Mt. Etna, there are no indications of alteration up to 240 °C but the samples alter quite dramatically for increasingly elevated temperatures up to 500 °C. Samples from La Palma do not show any alteration up to 300 °C. Even for higher temperatures, the signal is reversible within 5–10%. The Hawaiian samples are unaffected up to 300 °C; they show moderate signs of alteration for higher temperatures. For the La Palma and the Hawaiian sites, the magnetization-versus-temperature appears to be even reversible within 10–20% after heating the samples up to 720 °C. Site ET-23-2 shows a decrease in magnetic activity of approximately 30% after heating to 720 °C, while on the contrary, sites ET-71-3C, ET-79-1 and HW-14B reveal an increase of magnetic activity, especially around the temperatures normally used in paleointensity experiments.

The set temperatures of the MSP paleointensity experiments were selected based on the dominant Curie temperature, the alteration temperature and the percentage of the NRM that is demagnetized at the proposed set temperature (Table 2). In the progressive thermal demagnetization experiment, these temperatures unblock approximately 25% of the NRM for sites ET-23-2, ET-83-4A and LP-1; approximately 55% for ET-71-3C and ET-79-1; and just 10–15% for the Hawaiian sites.

4.3. Paleointensity results

All sites in this study yielded technically acceptable MSP-DSC results, although there is some variation in the quality of the data between sites (Fig. 5 and Table 3, the outcome of the MSP-DB experiments is shown in the Supplementary material). Sites ET-71-3C and HW-37 show very little spreading in the data points, yielding r^2 values well above 0.95. For sites with less data points (ET-23-2 and ET-79-1), the r^2 is generally quite high, but the one standard deviation uncertainty envelope around the line fit is rather wide.

All sites from Mt. Etna yield underestimated paleointensities with respect to the IGRF. Site ET-23-2 (24.3 μT [9.8–32.2 μT], with *x*-axis cut-offs of the one-standard-deviation uncertainty envelope between brackets) and ET-71-3C (25.8 μT [22.4–29.0 μT]) gave underestimates of more than 40%. The other two Etna sites, ET-79-1 and ET-83-4A, yielded slightly higher paleointensities (30.6 μT [12.9–40.5 μT] and 28.5 μT [21.0–36.4 μT], respectively), but still underestimates with IEFs of −30.6% and −36.4%. The La Palma site (34.1 μT [28.7–39.2 μT]) also yielded an underestimate with an IEF of −13.5%. The IGRF value of 39.4 μT, however, is only just outside one standard deviation of the observed paleointensity.

Two of the Hawaiian sites yield approximately correct estimates of the IGRF value: 35.9 μT [30.2–42.0 μT] with an IEF of only −0.8% for site HW-14B, and 38.2 μT [27.6–47.1 μT], a slight overestimate with an IEF of +5.5% for site HW-17B. The third Hawaiian site, HW-37, yields an underestimate of the IGRF: 25.8 μT [21.8–29.4 μT], with an IEF of −29.5%.

The rock-magnetic analyses used to determine the set temperature used in the MSP-DSC experiments indicate no chemical alteration in the samples. However, the MSP experiments fail to resolve the IGRF field within error for six out of the eight sites in this study.

4.4. ARM acquisition experiments

Samples from all sites were subjected to at least one of the ARM techniques described before. The aligned ARM acquisition protocol was applied to all Etna sites and the La Palma site; the Hawaiian sites were subjected to the single core protocol. Samples from site ET-79-1 underwent both protocols, which showed broadly the same behavior (Fig. 6c and d). Thus the assumptions made about the separability of NRM and ARM signals required for both methods, appear to be plausible.

For the two sites in this study for which the MSP-DSC protocol is able to resolve the expected paleointensity within a few percent (HW-14B and HW-17A), the ARM acquisition experiment on heated samples shows no change in behavior compared to the pristine samples (Fig. 6g and h). For the other six sites, which all yield underestimates of the paleofield, the ARM acquisition experiments indicate that the heated samples acquire more ARM when subjected to the same AF field than the pristine samples do. This change in acquisition behavior is most pronounced for intermediate AF levels between 10 and 80 mT. For all samples, except ET-23-2, the saturated ARM of the heated samples is within a few percent equal to the saturated ARM of the pristine samples.

Importantly, the observed changes in ARM acquisition behavior before and after heating at the set temperature are nearly always removed if the samples are fully AF demagnetized (three-axis at 300 mT) before subjecting them to the ARM acquisition experiments. Apparently, the changes in domain state induced by heating are removed by a full AF demagnetization. Site ET-23-2 is remarkable: after full AF demagnetization the subsequent ARM acquisition curve appears to be even more convex than that of the heated but not AF demagnetized samples. As an example, for an AF field of 20 mT the heated, AF demagnetized samples acquire 3.5 times the ARM of the AF demagnetized samples that were not heated. For the highest AF field used in the experiment on AF demagnetized samples (150 mT) the acquired ARM of the heated samples is almost twice the acquired ARM of the unheated samples. Because of these surprising results, all experiments on samples from site ET-23-2 were repeated with different samples from the same site, with the same outcome.

The severity of the changes in ARM acquisition behavior varies among sites. The results of site LP-1 (AL) and HW-37 (SC) show less

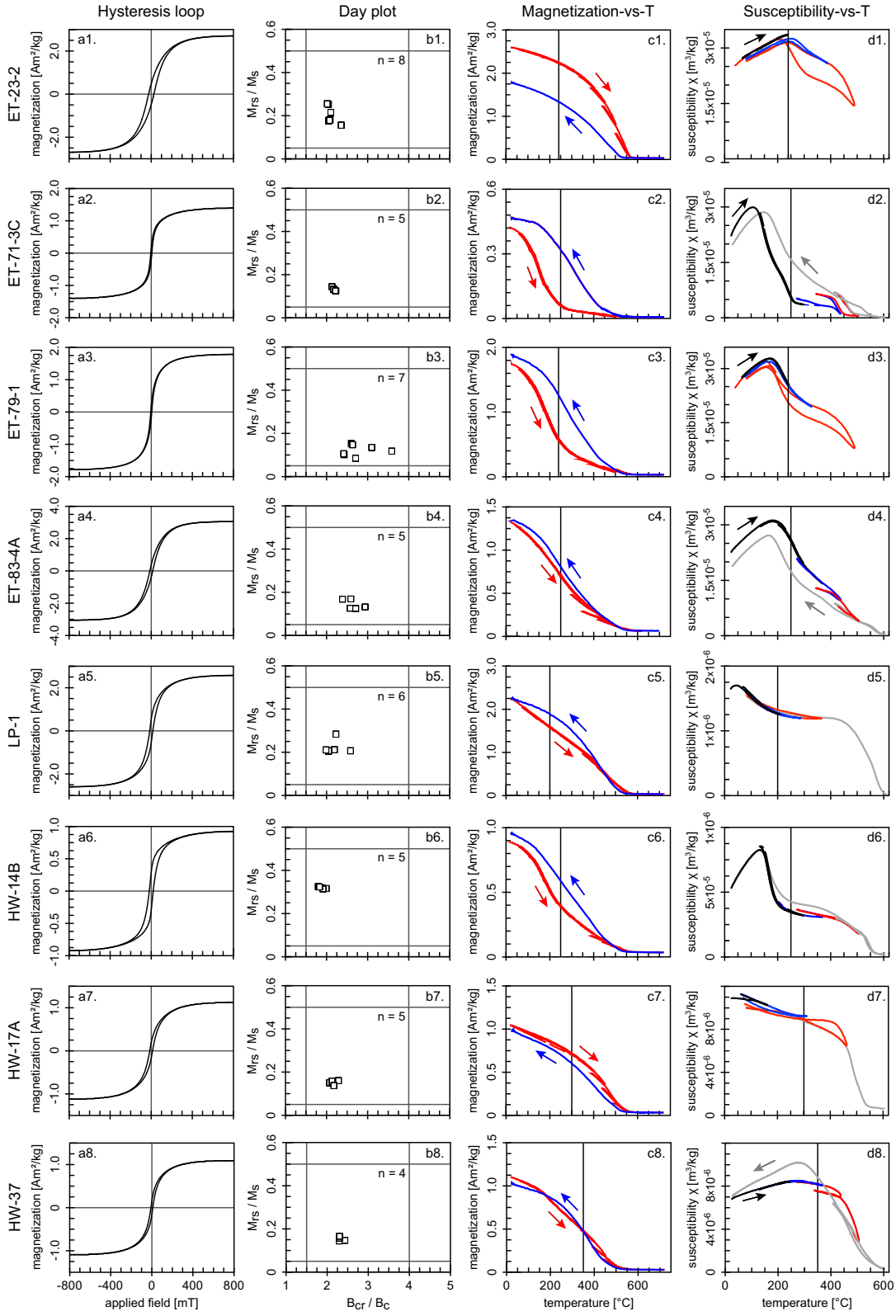

Fig. 4. Rock-magnetic analyses, for sample labels see Table 1. Typical hysteresis loops (a1–a8) all show PSD behavior, with ET-79-1 trending the most towards MD. Typical saturation magnetizations are ~1–2 Am^2/kg. In the Day plots (b1–b8) the number of samples is indicated, the Hawaiian sites show remarkably little scatter compared to the other sites. Scatter may be introduced by among-sample heterogeneities because of their small size: typically 2–6 mg. In both the magnetization-versus-temperature (c1–c8) and the susceptibility-versus-temperature (d1–d8) diagrams, the set temperature of the MSP experiment is indicated as a solid black line. Chemical alteration, indicated by a non-reversible cooling segment after a certain heating temperature, is best revealed by the susceptibility-versus-temperature experiments. In the magnetization-versus-temperature diagrams successive incremental heating cycles are indicated with the red line; an irreversible cooling segment testifies thermochemical alteration. The final cooling curve is indicated with a blue line. In the susceptibility-versus-temperature experiments reversible heating cycles are indicated with blue; the irreversible cycles are red, cycles to higher temperatures than the alteration temperature are indicated in gray. (For interpretation of the references to color in this figure legend, the reader is referred to the web version of this article.)

Table 2
Summary of the important parameters to determine the set temperature in the MSP paleointensity experiments.

Site	Dominant Curie T (°C)	Alteration T (°C)	MSP set T (°C)	Demagnetization at MSP set T (%)
ET-23-2	550	>250	240	25
ET-71-3C	240	>350	250	50
ET-79-1	300	>300	240	55
ET-83-4A	450	>350	250	30
LP-1	550	>300	200	25
HW-14B	200/450	>250	250	20
HW-17A	550	>300	300	10
HW-37	480	>390	350	10

From left to right: site, dominant Curie temperature (T), alteration temperature based on the rock-magnetic analyses (Figs. 3 and 4), the set temperature used in the MSP experiments and the percentage of the NRM that is demagnetized at the set temperature of the MSP experiments.

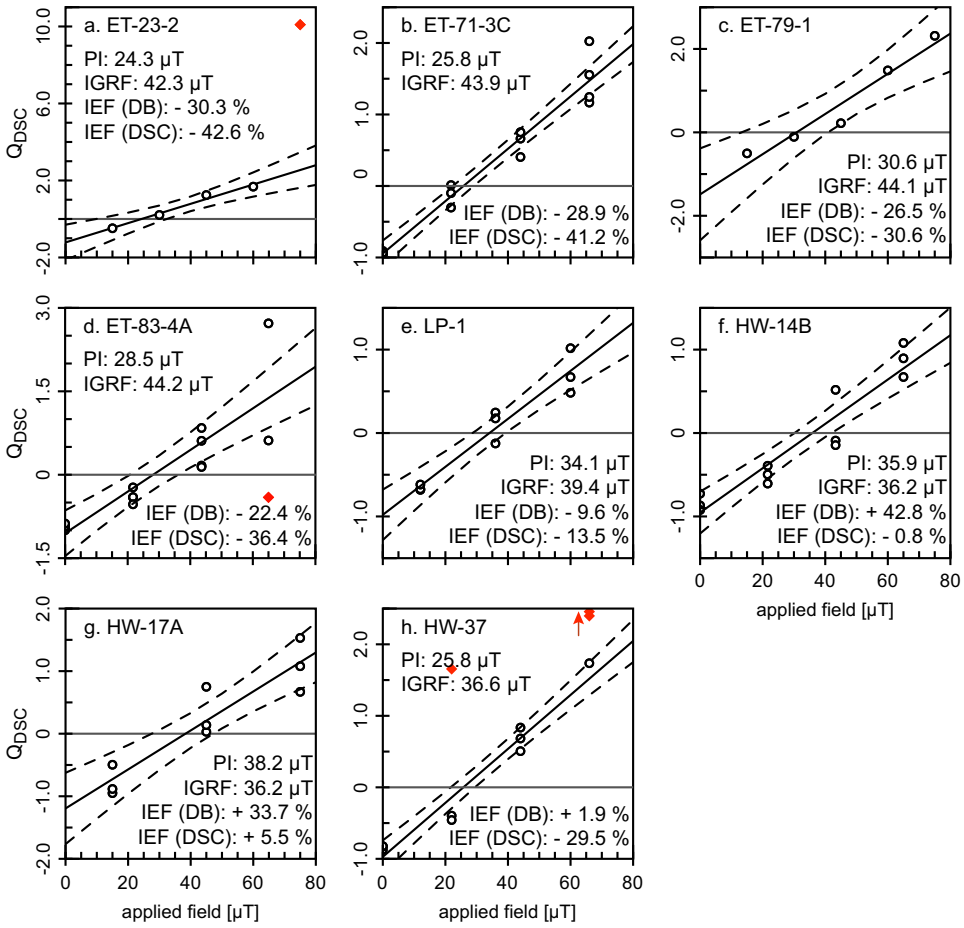

Fig. 5. MSP-DSC paleointensity results, for sample labels see Table 1. All eight sites yield technically acceptable MSP paleointensity plots, although the scatter in the data varies. The upper and lower boundaries of the error envelope of one standard deviation above and below the fit are depicted as dashed lines. Data points that are outside the error envelope of one standard deviation following from calculations including all data are rejected, and the fit and error envelope are recalculated omitting the rejected data points which are subsequently depicted as solid red diamonds. Number of samples used for the experiments: ET-23-2: 5 (1 rejected); ET-71-3C: 15; ET-79-1: 5; ET-83-4A: 16 (1 rejected); LP-1: 8; HW-14B: 12; HW-17A: 9; HW-37: 12 (3 rejected). The obtained paleointensity, the appropriate IGRF reference value and the intensity error fraction (IEF) of both the MSP-DB and the MSP-DSC protocols are indicated. (For interpretation of the references to color in this figure legend, the reader is referred to the web version of this article.)

alteration than the sites of Mt. Etna. Because of the small mass of the LP-1 samples in the aligned ARM experiment, the results were not very consistent among the samples. Therefore the experiment was repeated, so the results of eight samples can be considered for both groups of samples, which reduced inconsistency substantially. A single core experiment with bigger samples might have been insightful, because the noise probably would be significantly lower. Unfortunately, the amount of material still available after other experiments was not sufficient to perform a single core experiment on LP-1.

For site LP-1, the heated samples acquire approximately 50% more ARM than the untreated samples for the lowest AF fields (0–5 mT); for the intermediate AF fields (around 25 mT) the effect is approximately 30%; and for the full ARM (at 150 mT) the heated samples acquire only 6% more ARM than the untreated samples. Due to the number of samples needed because of the rather poor consistency among the samples in the aligned ARM acquisition experiment, less but ten times bigger samples were used for the experiment on fully AF demagnetized samples. These bigger samples showed much more consistency among samples and yielded

Table 3
Summary of the multispecimen (MSP) paleointensity results (see Dekkers and Böhnel, 2006 and Fabian and Leonhardt, 2010).

Site	PI (μT)	PI confidence interval (μT)	IEF (%)	*n* (rejected)	r^2	*a*	*b*	DSC-correction (μT)
MSP-DB								
ET-23-2	29.5	25.2–33.2	−30.3	5 (1)	0.997	0.0032	0.0652	
ET-71-3C	31.2	28.2–34.1	−28.9	15	0.966	0.0151	0.4713	
ET-79-1	32.4	30.3–34.5	−26.5	18	0.978	0.0170	0.5518	
ET-83-4A	34.3	26.5–44.2	−22.4	16 (1)	0.757	0.0081	0.2766	
LP-1	35.6	28.8–41.7	−9.6	8	0.907	0.0075	0.2670	
HW-14B	51.7	43.6–63.9	42.8	12	0.841	0.0037	0.1895	
HW-17A	47.7	39.4–58.4	33.7	27	0.729	0.0034	0.1620	
HW-37	37.3	35.1–39.7	1.9	12 (1)	0.985	0.0049	0.1815	
MSP-DSC								
ET-23-2	24.3	9.8–32.2	−42.6	5 (1)	0.979	0.0501	1.2179	−5.2
ET-71-3C	25.8	22.4–29.0	−41.2	15	0.960	0.0366	0.9441	−5.4
ET-79-1	30.6	12.9–40.5	−30.6	5	0.941	0.0484	1.4803	−1.8
ET-83-4A	28.5	21.0–36.4	−36.4	16 (1)	0.782	0.0370	1.0525	−5.8
LP-1	34.1	28.7–39.2	−13.5	8	0.924	0.0288	0.9804	−1.5
HW-14B	35.9	30.2–42.0	−0.8	12	0.901	0.0266	0.9535	−15.8
HW-17A	38.2	27.6–47.1	5.5	9	0.862	0.0312	1.1948	−9.5
HW-37	25.8	21.8–29.4	−29.5	12 (3)	0.954	0.0377	0.9719	−11.5

From left to right: site; obtained paleointensity (PI); paleointensity confidence interval (the *x*-axis cut-offs of the uncertainty envelope of one standard deviation above and below the fit); intensity error fraction (IEF) in % related to the respective IGRF value (Table 1); the number of samples used in the paleointensity experiments (number of rejected points between brackets); the r^2 of the fit, slope (a); intercept (b) and the DSC correction in μT. The upper block of data gives the MSP-DB results (for figures, see the Supplementary material), the MSP-DSC results are provided in the lower block (see Fig. 5).

a slightly different behavior: for the lower AF fields the ARM of the heated samples is slightly higher than the ARM of the unheated, AF demagnetized samples, approximately 25% for a field of 3 mT. Between 10 and 90 mT the ARM acquired by the untreated samples is higher than that of the heated, AF demagnetized samples, the difference is maximally 10% for an AF field of 35 mT. For the full ARM of 150 mT, the difference is equal to the difference in behavior of the samples that were not fully AF demagnetized prior to the ARM acquisition experiment: approximately 6%. So the total potential ARM capacity did not increase by the AF demagnetization of the samples, only the ARM capacity of intermediate AF fields seems to be affected.

5. Discussion

All sites included in this study should be suitable for paleointensity experiments. They involve recent lavas with univectorial demagnetization behavior towards the origin, with barely or no overprints. The rock-magnetic analyses show (small) PSD-size grains and indicate slight differences in Ti/Fe ratios of the magnetic particles. The thermal analyses do not indicate changes in magnetic properties for the temperatures used in the MSP paleointensity experiments. Nevertheless, the intensity error fractions obtained from the MSP-DSC experiments vary from −42.6% to +5.5%.

5.1. Effects of changes in magnetic state

Fabian and Leonhardt (2010) show by magnetic modeling that tail effects cause the MSP-DB method to yield overestimates of the paleofield, and that underestimates of the paleofield are thus not to be expected. The MSP-DSC protocol is designed to reduce or eliminate the predicted (and experimentally observed) overestimates in the MSP-DB experiments. Nevertheless, if samples suffer from changes in the configuration of their magnetic domain state, the outcome of MSP-style paleointensity protocols is unpredictable. A newly acquired domain configuration could possess a lower net magnetic moment than the original NRM configuration. Then those samples will have a lower remanence after reheating them in the same field as the original NRM was acquired in, thus increasing the obtained MSP paleointensity estimate. If the new domain configuration has a higher net magnetic moment, the composite remanence of the samples will increase, lowering the obtained MSP paleointensity. Tail effects will still be present in the new domain state configuration. Apparently, all sites included in this study, except sites HW-14B and HW-17A, change their domain state to a configuration that lowers the MSP outcomes. Site HW-37 is particularly misleading: the MSP-DB protocol would yield the correct answer (IEF of 1.9%) while the tail correction of the MSP-DSC protocol yields an underestimate of 29.5%. The change in the domain state that lowers the obtained paleointensity fortuitously must be approximately equal to the tail effect that increases the obtained paleointensity. Therefore the MSP-DB paleointensity seems to yield the proper results, while the tail corrected outcome of the MSP-DSC protocol yields the observed underestimate of 29.5%.

5.2. ARM acquisition curves and detecting changes in magnetic state

Here we evaluate the performance of the ARM acquisition experiments in relation to paleointensity results to assess their capability to reveal information on changes in magnetic domain configuration after heating. This comparison inherently is based on the premise that ARM and TRM are analogous, a property that has been exploited before (see Section 3.4.1). As dealt with earlier on in that section, ARM acquisition curves are able to visualize minute changes in magnetic state – either caused by thermochemical or by magnetic alteration (i.e. changes in domain structure). This is because ARM has a high resolving power particularly in the grain-size realm straddling the SD size. Since subtle magnetic alteration may well be dependent on the magnetic starting state of the particles, ARM acquisition curves were determined on 'pristine' starting states (either the NRM state or a thermally treated state during the paleointensity experiment in case of the heated samples) and on the AF-demagnetized starting state. For all sites of this study, the ARM acquisition experiments are capable of qualitatively indicating changes in domain state; with the related implications for the obtained paleointensity results. This highlights that the ARM-TRM analogy is reasonable. However, the variation in behavior of ARM acquisition curves among the sites and the differences in severity of the changes currently impede a more quantitative correction of the obtained paleointensities based on the ARM acquisition techniques presented in this

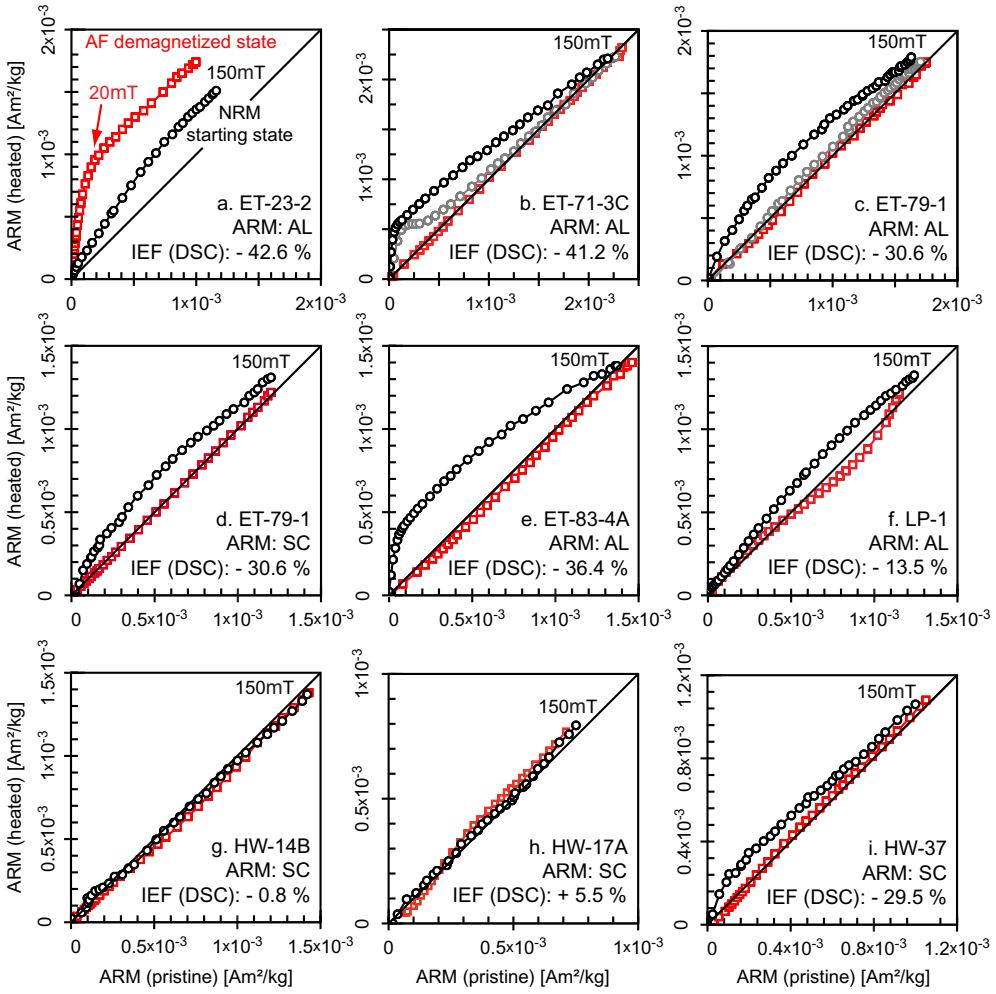

Fig. 6. Results of ARM acquisition experiments, for sample labels see Table 1. ARM acquisition experiments with samples in their NRM state are indicated as black circles, repeated experiments on the same samples in their AF demagnetized state (three axis, 300 mT) are indicated in red squares. A few small samples of sites ET-71-3C and ET-79-1 showed much weaker coercivity behavior than the bulk samples of those sites (sometimes demagnetized down to 5% of the NRM for an AF field of 10 mT, were sister specimens and the bulk behavior holds approximately 60% of the NRM at 10 mT), possibly due to the combination of the heterogeneity of the samples and the sample size in the aligned ARM acquisition experiments. These samples were omitted from the ARM acquisition curves in black, but are included in the gray ARM curves. The highest ARM acquisition AF field used in the experiments is 150 mT. The applied ARM acquisition technique (aligned (AL) or single core (SC)) and the intensity error fraction (IEF) of the obtained paleointensity from the MSP-DSC experiment are indicated. Both ARM acquisition protocols were applied to samples of ET-79-1, yielding comparable results. The number of samples used per experiment: ET-23-2 and LP-1: eight parallel, eight antiparallel for both the pristine and heated series; ET-71-3C, ET-79-1 AL and ET-83-4A: four parallel, four antiparallel for both the pristine and heated series; ET-79-1 SC: four in both the 0- and the 35-μT-series for the heated samples, three in both series for the pristine samples; HW-14B, HW-17A and HW-37: three in both series, for the pristine and heated samples. Sites HW-14B and HW-17A do not show any change in their ARM acquisition behavior after heating or after full AF demagnetization of the samples. Samples from all other sites acquire more ARM after heating for the same AF field, especially for intermediate AF fields (around 30 mT). (For interpretation of the references to color in this figure legend, the reader is referred to the web version of this article.)

paper. Predicting precisely how the domain state would change and how such changes would correlate to changes in ARM acquisition behavior is hard at present.

It is noteworthy that the ARM diagrams of Fig. 6 are rather conservative in indicating changes in acquisition behavior: sample HW-37 for example (Fig. 6i) acquires 75% more ARM after heating for the low AF field values around 5 mT, decreasing towards 25% for an AF field of 15 mT and a still significant 15% for the intermediate AF fields around 30 mT. For a sample identified as 'indicating no change', HW-17A for example, the heated and pristine ARM acquisitions differ less than 5% for the intermediate AF fields. In a sense the diagrams are subtle.

5.3. Comparison of ARM acquisition curves of the NRM and AF-demagnetized starting states

The ARM acquisition observations presented are conform their underestimated paleointensities. The repeated ARM acquisition experiment after a full AF demagnetization generally undoes the earlier observed changes in ARM acquisition behavior (site ET-23-2 is an exception). This indicates that the alteration is of magnetic origin and not caused by subtle thermochemical processes. Site ET-23-2 (with a large paleointensity underestimate) has a remarkable ARM behavior. The pristine state behaves in line with its expectation by showing a higher ARM after heating. AF demagnetization even enhances this behavior making it unclear whether only magnetic, only thermochemical, or combined magnetic and thermochemical effects play a role. It may be clear, however, that the obtained paleointensity estimate is subject to doubt and represents an underestimate. Hence, AF-demagnetization of samples before the ARM acquisition experiment must be avoided to be able to evaluate whether or not changes in magnetic domain configuration have occurred during the laboratory heating of the paleointensity experiment. The assessment must be based on differences in ARM acquisition behavior between heated and pristine samples that have not been AF-demagnetized.

5.4. The MSP-DSC protocol

The set of observations from the present study suggests that the MSP-DSC protocol is able to fully or at least largely correct for the magnetic tail effects introduced by heating samples. As stated before, if the domain configuration changes during the experiments, the outcome of the paleointensity experiment depends on the newly acquired domain configuration being more or less 'efficient' than the original domain state of the NRM. The six flows subject of this study that do not yield an approximately correct paleointensity, all yield underestimated paleointensities that are corrected for tail effects. Note that at the respective set temperature no indications of chemical alterations are present. This implies that the pTRMs imparted during the MSP-DSC experiments are locked-in in a different domain configuration than that of the NRM state.

Based on the observations presented in this study, the detailed ARM acquisition experiments on pristine samples are capable of detecting changes in the configuration of the domain state and can therefore label obtained MSP-DSC paleointensities as being an underestimate, or approximately correct. If allowed by the constraints posed by the necessary unblocked fraction of the NRM for MSP-style experiments and indications of chemical alteration from rock-magnetic experiments, testing multiple temperatures for alterations in magnetic domain configuration and selecting the temperature for which the least or no alteration is observed as set temperature for the MSP-DSC protocol may significantly increase the success rate of the paleointensity experiments. Besides testing multiple temperatures for one site, testing different sites from the same cooling unit also may provide better constraints on the paleointensity, since sites from the same cooling unit may vary in rock-magnetic properties.

6. Conclusion

Absolute paleointensity methods suffer from chemical alterations and changes in magnetic domain state due to heating. This makes the assessment of a suitable temperature or temperature range in which these alterations do not occur in the samples prior to the paleointensity experiment very important. Chemical alterations are generally well detected by rock-magnetic experiments such as the measurement of magnetization and susceptibility as a function of temperature, but changes in magnetic domain state often go undetected.

The MSP-DSC protocol of Fabian and Leonhardt (2010) corrects for domain state and tail effects and lowers the paleointensity estimates of the MSP-DB protocol. In this study the MSP-DSC protocol yields approximately correct (or slightly overestimated) paleointensities and underestimates of the paleofield. For all sites included in this study, the ARM acquisition experiments as described above are capable of discriminating between the underestimates and approximately correct values. We suggest an optimized workflow for a paleointensity experiment, combining the MSP-DSC protocol with ARM acquisition checks as follows:

1. A progressive thermal demagnetization experiment.
2. Rock-magnetic analyses to determine the chemical alteration temperature.
3. Select (a) potential set temperature(s) for the MSP-DSC protocol avoiding chemical alteration, while unblocking a significant amount of the NRM.
4. Conduct one of the ARM acquisition experiments presented in this paper, testing the potential set temperature(s), preferably using the single core protocol.
5. Follow the MSP-DSC protocol (Fabian and Leonhardt, 2010), using the set temperature with the least or no observed alteration in the ARM acquisition experiments of step 4.

This workflow assesses the best set temperature for the MSP-DSC protocol independently of – and prior to – the paleointensity experiment. Furthermore, the outcome of the MSP-DSC experiment can be labeled as being approximately correct or an underestimate of the paleofield independently of the obtained paleointensity.

Acknowledgements

We thank Andy Biggin for his help in the field on Mt. Etna and for his helpful comments and discussions. We are grateful for the comments of Yongjae Yu and an anonymous reviewer, which greatly helped to improve the manuscript. This research was funded by a grant from the Earth and Life Science Division (ALW) of the Netherlands Organization for Scientific Research (NWO). The robotized 2G SQUID magnetometer was developed with support of the instrument fund of the Netherlands Organization for Scientific Research and the AGICO JR6 spinner magnetometer was acquired with support from ISES, the Netherlands Research Centre for Integrated Solid Earth Science.

Appendix A. Supplementary data

Supplementary data associated with this article can be found, in the online version, at doi:10.1016/j.pepi.2012.01.006.

References

Biggin, A.J., Perrin, M., Dekkers, M.J., 2007a. A reliable absolute palaeointensity determination obtained from a non-ideal recorder. Earth and Planetary Science Letters 257 (3–4), 545–563.
Biggin, A.J., Perrin, M., Shaw, J., 2007b. A comparison of a quasi-perpendicular method of absolute palaeointensity determination with other thermal and microwave techniques. Earth and Planetary Science Letters 257 (3–4), 564–581.
Böhnel, H., Herrero-Bervera, E., Dekkers, M.J., 2011. In: Petrovský, E. et al. (Eds.), The Earth's Magnetic Interior. Springer, Dordrecht, Netherlands.
Brown, M.C., Gratton, M.N., Shaw, J., Holme, R., Soler, V., 2009. Microwave palaeointensity results from the Matuyama–Brunhes geomagnetic field reversal. Physics of the Earth and Planetary Interiors 173 (1–2), 75–102.
Calvo, M., Prévot, M., Perrin, M., Riisager, J., 2002. Investigating the reasons for the failure of palaeointensity experiments: a study on historical lava flows from Mt. Etna (Italy). Geophysical Journal International 149 (1), 44–63.
Coe, R.S., 1967. The determination of paleo-intensities of the Earth's magnetic field with emphasis on mechanisms which could cause non-ideal behavior in Thellier's method. Journal of Geomagnetism and Geoelectricity 19, 157–178.
Coe, R.S., 1978. Geomagnetic paleointensities from radiocarbon-dated lava flows on Hawaii and the question of the Pacific nondipole low. Journal of Geophysical Research 83, 1740–1756.
Cottrell, R.D., Tarduno, J.A., 1999. Geomagnetic paleointensity derived from single plagioclase crystals. Earth and Planetary Science Letters 169, 1–5.
Day, R., Fuller, M., Schmidt, V., 1977. Hysteresis properties of titanomagnetites: grain-size and compositional dependence. Physics of the Earth and Planetary Interiors 13, 260–267.
Dekkers, M.J., Böhnel, H.N., 2006. Reliable absolute palaeointensities independent of magnetic domain state. Earth and Planetary Science Letters 248 (1–2), 508–517.
Dunlop, D., Özdemir, Ö., 1997. Cambridge Studies in Magnetism: Rock Magnetism: Fundamentals and Frontiers. Cambridge University Press, Cambridge, UK.
Fabian, K., Leonhardt, R., 2010. Multiple-specimen absolute paleointensity determination: an optimal protocol including pTRM normalization, domain-state correction, and alteration test. Earth and Planetary Science Letters 297 (1–2), 84–94.
Herrero-Bervera, E., Valet, J.-P., 2009. Testing determinations of absolute paleointensity from the 1955 and 1960 Hawaiian flows. Earth and Planetary Science Letters 287 (3–4), 420–433.
Hill, M.J., Shaw, J., 2000. Magnetic field intensity study of the 1960 Kilauea lava flow, Hawaii, using the microwave palaeointensity technique. Geophysical Journal International 142, 487–504.
Hill, M.J., Shaw, J., 1999. Palaeointensity results for historic lavas from Mt. Etna using microwave demagnetization/remagnetization in a modified Thellier-type experiment. Geophysical Journal International 139 (2), 583–590.
Inoue, S., Yamazaki, T., 2010. Geomagnetic relative paleointensity chronostratigraphy of sediment cores from the Okhotsk Sea. Palaeogeography, Palaeoclimatology, Palaeoecology 291 (3–4), 253–266.
Johnson, H.P., Lowrie, W., Kent, D.V., 1975. Stability of anhysteretic remanent magnetization in fine and coarse magnetite and maghemite particles. Geophysical Journal of the Royal Astronomical Society 41, 1–10.
Kono, M., Ueno, N., 1977. Paleointensity determination by a modified Thellier method. Physics of the Earth and Planetary Interiors 13 (4), 305–314.

Krasa, D., Heunemann, C., Leonhardt, R., Petersen, N., 2003. Experimental procedure to detect multidomain remanence during Thellier–Thellier experiments. Physics and Chemistry of the Earth 28, 681–687.
Leonhardt, R., Hufenbecher, F., Heider, F., 2000. High absolute paleointensity during a mid Miocene excursion of the Earth's magnetic field. Earth and Planetary Science Letters 184, 141–154.
Lowrie, W., Fuller, M., 1971. On the alternating field demagnetization characteristics of multidomain thermoremanent magnetization in magnetite. Journal of Geophysical Research 76, 6339–6349.
Mankinen, E.A., Champion, D.E., 1993. Latest Pleistocene and Holocene geomagnetic paleointensity on Hawaii. Science 262 (5132), 412.
Meynadier, L., Valet, J.-P., Weeks, R., Shackleton, N.J., Hagee, V.L., 1992. Relative geomagnetic intensity of the field during the last 140 ka. Earth and Planetary Science Letters 114 (1), 39–57.
Mullender, T.A.T., van Velzen, A.J., Dekkers, M.J., 1993. Continuous drift correction and separate identification of ferromagnetic and paramagnetic contributions in thermomagnetic runs. Geophysical Journal International 114, 663–672.
Muxworthy, A.R., 2010. Revisiting a domain-state independent method of palaeointensity determination. Physics of the Earth and Planetary Interiors 179 (1–2), 21–31.
Riisager, P., Riisager, J., 2001. Detecting multidomain magnetic grains in Thellier palaeointensity experiments. Physics of the Earth and Planetary Interiors 125, 111–117.
Rolph, T.C., Shaw, J., 1985. A new method of palaeofield magnitude correction for thermally altered samples and its application to Lower Carboniferous lavas. Geophysical Journal of the Royal Astronomical Society 80, 773–781.
Shaw, J., 1974. A new method of determining the magnitude of the paleomagnetic field. Geophysical Journal of the Royal Astronomical Society 39, 133–141.
Speranza, F., Branca, S., Coltelli, M., D'Ajello Caracciolo, F., Vigliotti, L., 2006. How accurate is "paleomagnetic dating?" New evidence from historical lavas from Mount Etna. Journal of Geophysical Research – Solid Earth 111 (B12), B12S33.
Tanguy, J.C., 1975. Intensity of the geomagnetic field from recent Italian lavas using a new paleointensity method. Earth and Planetary Science Letters 27, 314–320.
Tauxe, L., Staudigel, H., 2004. Strength of the geomagnetic field in the Cretaceous Normal Superchron: new data from submarine basaltic glass of the Troodos Ophiolite. Geochemistry, Geophysics, Geosystems 5 (2).
Thellier, E., Thellier, O., 1959. Sur l'intensité du champ magnétique terrestre dans le passé historique et géologique. Annales de Geophysique 15, 285–378.
Tsunakawa, H., Shaw, J., 1994. The Shaw method of palaeointensity determinations and its application to recent volcanic rocks. Geophysical Journal International 118, 781–787.
Valet, J.-P., Soler, V., 1999. Magnetic anomalies of lava fields in the Canary islands. Possible consequences for paleomagnetic records. Physics of the Earth and Planetary Interiors 115, 109–118.
Valet, J.-P., Herrero-Bervera, E., Carlut, J., Kondopoulou, D., 2010. A selective procedure for absolute paleointensity in lava flows. Geophysical Research Letters 37 (L16308).
Valet, J.P., Meynadier, L., 1993. Geomagnetic field intensity and reversals during the past four million years. Nature 366, 234–238.
Xu, S., Dunlop, D., 1995. Toward a better understanding of the Lowrie–Fuller test. Journal of Geophysical Research 100, 22533–22542.
Yamamoto, Y., Tsunakawa, H., 2003. Palaeointensity study of the Hawaiian 1960 lava: implications for possible causes of erroneously high intensities. Geophysical Journal International 153, 263–276.
Yamazaki, T., Kanamatsu, T., Mizuno, S., Hokanishi, N., Gaffar, E.Z., 2008. Geomagnetic field variations during the last 400 kyr in the western equatorial Pacific: paleointensity-inclination correlation revisited. Geophysical Research Letters 35 (20).